

Charge-transport and photocurrent generation in bulk hetero junction based on Chloro-aluminum phthalocyanine (ClAlPc) and Rose Bengal (RB)

M. S. Roy · P. Balraju · Y. S. Deol ·
S. K. Sharma · G. D. Sharma

Received: 27 February 2008 / Accepted: 18 June 2008 / Published online: 9 July 2008
© Springer Science+Business Media, LLC 2008

Abstract Bulk-hetero junctions were made with the intermixing of Chloro-aluminum phthalocyanine (ClAlPc) (p-type) and Rose Bengal (RB) (n-type material) from the common solvent. The optical properties of blend reveal that light harvesting is possible from almost entire visible spectrum of the material. The devices were characterized by recording its J - V in dark and under illumination and impedance analysis under various temperatures over wide frequency range, i.e., from 100 Hz to 1 MHz. Various photovoltaic parameters like open circuit voltage (V_{oc}), short-circuit photocurrent (J_{sc}), and fill factor were evaluated and found to be as 0.92 V and 0.44 mA/cm² and 0.48, respectively. Also, the effect of thermal annealing on the optical, electrical, and photovoltaic properties of bulk heterojunction device was investigated. From the impedance spectroscopy, we conclude that the change in bulk resistance and dielectric constant of active layer due to the illumination has a direct relevance to the photocurrent generation by the device. The overall observation reveals that upon thermal annealing of the device imparts substantial increase in hole mobility which results in balanced charge transport.

Introduction

In the past decades, interest on organic photovoltaic (OPV) devices has increased and several reviews on OPV have been published [1, 2]. The OPV offers low cost, low temperature solution processing, flexible substrates, and a high speed of processing. Several research groups have reported the synthesis and the use of materials which absorbs light with wavelengths above 600 nm in OPV's. Furthermore, organic semi-conducting materials in thin film form show high absorption coefficients exceeding 10⁵ cm⁻¹, which make them good chromophores for optoelectronics applications [3]. Organic materials having delocalized π electron system can absorb sunlight, create photo generated charge carriers, and transport these carriers toward the electrodes. Research on organic solar cells generally focuses either on solution processable organic semiconducting molecules/polymers or on vacuum-deposited small molecular materials [4, 5]. In recent years, the efficiency of OPV has been improved up to >5% [6, 7].

The initial step of photo carrier generation in OPV is exciton formation due to photon absorption by the active layer used in the device. In order to achieve the efficient OPVs, the exciton has to be dissociated at a donor-acceptor (D-A) interface into free charge carriers, which are subsequently collected at their respective electrodes. One limitation of OPVs is overlap between the active layer absorption with the solar spectrum. Indeed, over 60% of the total solar flux is at wavelength $\lambda > 600$ nm with $\sim 50\%$ in red and near infrared (NIR) spectrum at $600 < \lambda < 1,000$ nm. Therefore, new materials need to be developed and investigated that can absorb NIR radiation and effectively convert absorbed photons into the current. The OPV devices based on polymers sensitive to NIR

G. D. Sharma—on sabbatical leave from JNV Unuiversity, Jodhpur.

M. S. Roy · Y. S. Deol
Defence Laboratory, Jodhpur 342011, India

P. Balraju · S. K. Sharma · G. D. Sharma (✉)
Physics Department, Molecular Electronic and Optoelectronic
Device Laboratory, JNV University, Jodhpur 342005, India
e-mail: sharmagd_in@yahoo.com

Present Address:
G. D. Sharma
Mandsaur Institute of Technology, Mandsaur, MP, India

radiation up to $\lambda = 1,000$ nm have achieved a power conversion efficiency of 0.7% [8, 9].

It is widely recognized that efficient exciton dissociation occurs at the interface between donor (D) and acceptor (A) materials, but the short exciton diffusion lengths in organic limits conversion efficiency [10–12]. This issue has been addressed in molecular systems by improvements in materials selection [13–16]. Mixing technique such as blending of two different types semiconducting is commonly used in polymeric systems for creating a nanostructure interface with a high interfacial area between the donor and the acceptor species [17–21], with considerable efforts being directed to optimize the blend morphology and percolation between D and A domains. Postproduction heat treatments have also been investigated on spin-coated polymer blends to enhance crystallization of photoactive polymers, and thereby increasing the mobility of charge carriers [22]. In addition to that, thermal annealing has also been employed to induce the phase mixing in a bulk heterojunction polymer: fullerene structure [23], resulting in an improved D–A interface with better photovoltaic performance of the device.

However, bulk heterojunction photovoltaic devices based on small molecule organic materials have not been investigated extensively so far, even through an early attempt at mixing evaporated perylene and phthalocyanine films in double layer structure lead to a twofold increases in photovoltaic device efficiency [24]. The bulk heterojunction based on small molecules has been investigated on the structures containing co-deposited phthalocyanine and C_{60} either directly sandwiched contacts or in conjunction with continuous layer of different compositions [25–28]. Peumans et al. [12] employed the strained thermal annealing process on mixed vacuum deposited small molecular system, allowing for the formation of an interpenetrating D–A network and reported almost double power conversion efficiency over a bi-layer structure utilizing same materials. Recently, Chen et al. [29] reported an effective approach to improve the spectral coverage by simply doping a suitable fluorescent dye into the donor and/or the acceptor layer, upon doping the device CuPc/ C_{60} OPV device with 5,6,11,12-traphenylphthalene (rubrene), resulted in a high 5.58% power conversion efficiency, under an illumination intensity of 100 mW/cm².

As in nature, porphyrins are among the pigments most frequently employed as light harvesting antenna [30–33]. They efficiently utilize the absorbed energy to an acceptor site, where energy conversion takes place. Pcs [34, 35] are synthetic porphyrin analogues that exhibit particularly intense absorption in the red/NIR spectral region, where porphyrin fails to exhibit appreciable absorptions. Therefore, Pcs emerge as attractive molecular building blocks for the incorporation into D–A ensembles [36, 37], where they

function as antenna with both a wider absorbing range of the solar terrestrial spectrum.

In this paper, we have investigated the optical, electrical, and photovoltaic properties of bulk heterojunction fabricated from Chloro-aluminum phthalocyanine (CIAIPc) (p-type) and Rose Bengal (RB) (n-type material) in the form of blend device. The enhancement in power conversion efficiency upon thermal annealing is due to the increase in carrier mobility and modification of barrier formed with the electrode. This modification leads to an improvement in the collection of charge carriers by the electrodes and reduced recombination. The impedance measurements have also been used to correlate the change in impedance and dielectric constant upon the illumination with the short-circuit photocurrent.

Experimental procedure

Synthesis of materials

The material was synthesized through microwave-assisted synthesis process using focused microwave-based SYNTHEWAVE-402 (make Prolabo, France). In the procedure, the fine grounded phthalic anhydride (18 mmol), urea (92 mmol), ammonium chloride (17 mmol), ammonium molybdate (5 mg as catalyst), and aluminum chloride (0.6 mmol) were taken in a Quartz cylindrical reaction vessel (cap. 250 mL) and then irradiated with microwave (Power 300 W) under the given temperature profile. The product obtained within 10 min reaction time was washed with hot water and then dried in vacuum oven for 1 h. The re-precipitation through concentrated H_2SO_4 leads to the purest form of the material. Further, purification was carried out by Soxhlet extraction with acetone for 3 h and then pure M-Pc was obtained approximately in 70% yield. The material synthesized in this way is CIAIPc derivative which is soluble in organic solvents such as DMSO and DMF. RB is a well known n-type commercially available dye procured from Aldrich Chemicals, USA, and used as such without further purification. The molecular structure of CIAIPc and RB is shown in Fig. 1. For recording the absorption spectra and fluorescence spectra (FL), thin film of CIAIPc, RB, and CIAIPc:RB blend was spin cast from its solution in DMF onto the plane glass substrate. The absorption of the material was recorded using Photo Diode Array (Analytic Jena, Germany). The FL spectrum of the materials was recorded using Hitachi fluorescence spectrophotometer (F-3000). Cyclic voltammetry was carried out with a potentiostat–galvanostat (PGSTAT 30, Autolab, Eco-Chemie, Netherlands), a three-electrode system consisted of a gold working electrode, a platinum wire counter electrode, and a saturated calomel reference electrode

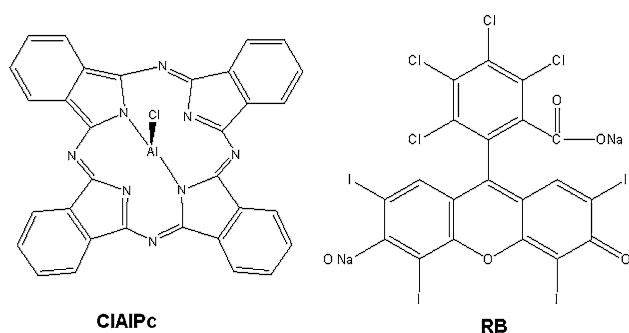


Fig. 1 Molecular structure of CIAIPc and RB

(SCE). CV was recorded in distilled DMF solvent using 0.1 M KCl as supporting electrolyte at a scan rate of 60 mV/s.

Fabrication of thin film device

CIAIPc was blended thoroughly with RB in (1:1 ratio) by grinding in mortar and then the device was fabricated by developing a thin-film of blend employing spin-coating technique over indium tin oxide (ITO)-coated glass substrate using DMF as solvent. For developing the film through spin-coating technique the rotation speed was initially kept at 100 rpm and then slowly and slowly accelerated to 1,000 rpm. The thickness of the film was evaluated through the spectral transmittance characteristics of the material and refractive index data. With the help of these two parameters and thickness monitor software provided with Photodiode array spectrophotometer (Analytic Jena, Germany), the actual thickness of the film was determined. The thickness of the film was about 200 nm. The layer is then heated in an oven at 60 °C for 30 min to remove the residual of the solvent. The silver (Ag) contact was then made over the top of the organic film covering 1 cm² active area of the device and configuration of the device is shown in Fig. 2. The *J*–*V* characteristics of the devices were measured with a Semiconductor Parameter Analyzer (HP 4145B) in dark and under illumination. The illumination was given by halogen lamp through ITO side and the light intensity was 10 mW/cm². Temperature

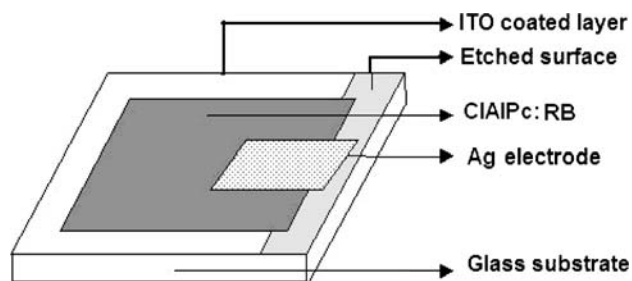


Fig. 2 Structure of Ag/CIAIPc:RB/ITO device

dependence of the impedance characteristics was recorded using FRA software (auto 30) in the range 300–370 K by controlling the temperature with the help of a temperature controller and monitoring it by digital temperature monitor. The developed films were annealed at 80 and 100 °C temperature in vacuum oven for 30 min. The film was then removed and kept in desiccator and temperature was brought down to room temperature.

Results and discussion

Optical studies

The UV–Visible spectra of the spin-coated CIAIPc and RB are shown in Fig. 3. It can be seen that CIAIPc absorbs light in 550–800 nm region and the acceptor material RB absorb in the wavelength region 400–600 nm. Hence, the combination of CIAIPc with acceptor material absorbs most of the solar energy spectrum in visible region. The RB has strong absorption feature as long as the absorption of the CIAIPc is weak or nonexistent. Therefore, the intermixing of these materials can be used as acceptor materials to form the bulk hetero-junction with CIAIPc. Absorption spectra of the blended film are shown in Fig. 3. It can be seen from this figure that the RB blended with CIAIPc in bulk heterojunction solar cells provides good coverage of solar spectrum and it is just a simple superposition of the two components used indicating that there is no ground-state interaction between the donor and the acceptor.

Electrochemical properties

The HOMO and LUMO energy levels of the donor and acceptor components for photovoltaic devices are very

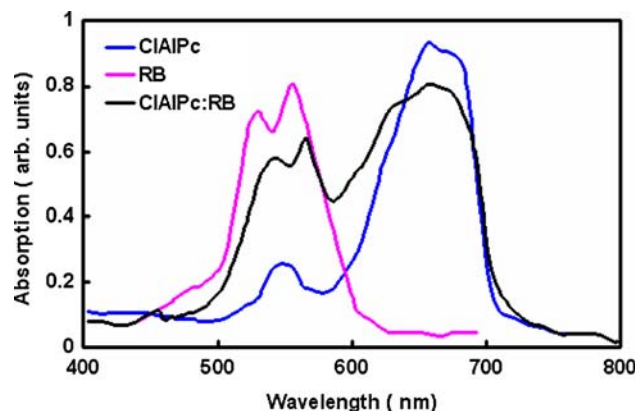


Fig. 3 Absorption spectra of CIAIPc, RB, and CIAIPc:RB blend thin films

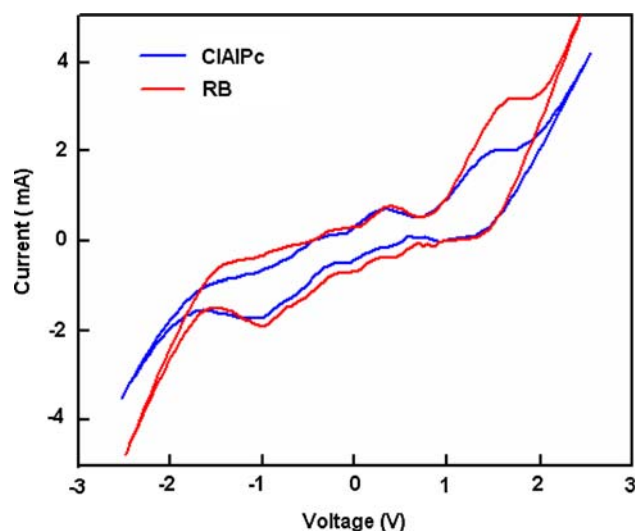


Fig. 4 Cyclic voltammogram of CIAIPc and RB

important factors to determine effective charge transfer between donor and acceptor. Cyclic voltammogram has proven to be a useful tool to determine the HOMO and LUMO levels in organic materials. Figure 4a and b shows the cyclic voltammograms of CIAIPc and RB, respectively. The evaluation of HOMO and LUMO levels has been done according to the following expressions [38].

$$E_{\text{HOMO}}(\text{eV}) = -E^{\text{ox}} - 4.34 \text{ eV}, \quad (1a)$$

$$E_{\text{LUMO}}(\text{eV}) = -E^{\text{red}} - 4.34 \text{ eV}, \quad (1b)$$

where E^{ox} and E^{red} are the measured oxidation and reduction potentials, respectively, relative to SCE. It is reported that the HOMO and LUMO of the organic semiconductors are highly localized on donor and acceptor moieties, respectively [39]. Table 1 shows the UV–Visible absorption data for materials and their cyclic voltammetric data. The obtained energy band gap estimated from CV is quite close to that extrapolated from absorption onset, i.e., optical energy band gap, which demonstrates the reliability of the electrochemical evaluation of LUMO and HOMO energy levels. In Fig. 5, the reduction and oxidation processes of CIAIPc:RB blended films are shown. In reduction cycle, the CIAIPc blended with RB exhibits reduction, i.e., n-doping and reduction peak shifted to higher potential with respect to those found for CIAIPc. In oxidation cycle, an irreversible

Table 1 Position of LUMO and HOMO levels and band gap calculated from the electrochemical and optical spectra of CIAIPc and RB

Material	E_{LUMO} (eV)	E_{HOMO} (eV)	E_{g} (Electro) (eV)	E_{g} (optical) (eV)
CIAIPc	-3.2	-4.9	1.7	1.66
RB	3.92	-5.98	2.06	1.98

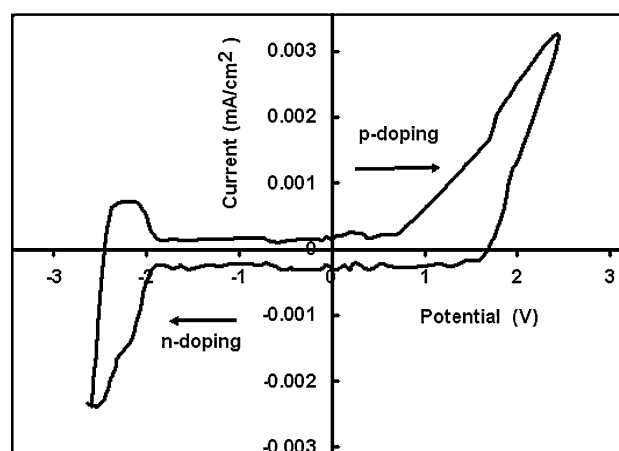


Fig. 5 Cyclic voltammogram of CIAIPc and RB blend

p-doping is observed and oxidation peak, shifted to higher potential as compared with that for CIAIPc alone. The shift to higher potentials of both oxidation and reduction cycles suggests a lower ionic conductivity and/or slower ionic motion in the blend film with respect to that in pure CIAIPc [40]. Since, the absorption spectra from D–A composite film are algebraic sum of the spectra of individual components. This suggests that charge transfer complex does not form in the blend.

The relative position of HOMO and LUMO with CIAIPc makes it possible to fabricate bulk heterojunction device. Fluorescence (FL) measurement technique was used to investigate the photo-induced charge generation in the blend of D–A. The photo-excited exciton passes through several processes:

- Recombination within donor or at the donor/acceptor interface.
- Energy transfer between the materials followed by radiative or nonradiative recombination.
- Charge transfer (exciton dissociation) at the D/A interface.

The measurements of fluorescence were made on a thin CIAIPc (D) film and compared with the FL of blend film from D–A (CIAIPc:RB). The FL spectra of the blends and donor (CIAIPc) are shown in Fig. 6. For the efficient photo-induced charge transfer, the relative position of donor LUMO and acceptor LUMO is crucial. The HOMO of CIAIPc is clearly higher in energy than HOMO of acceptor (RB). For the initiation of a photo-induced charge transfer process, the binding energy of the photogenerated excitons should be smaller than the difference between the electron affinities of the participating donor and acceptor species [10, 41]. The magnitude of exciton binding energy in most of the organic semiconductors is about 0.5 eV [42]. This value is comparatively smaller than that of the difference in

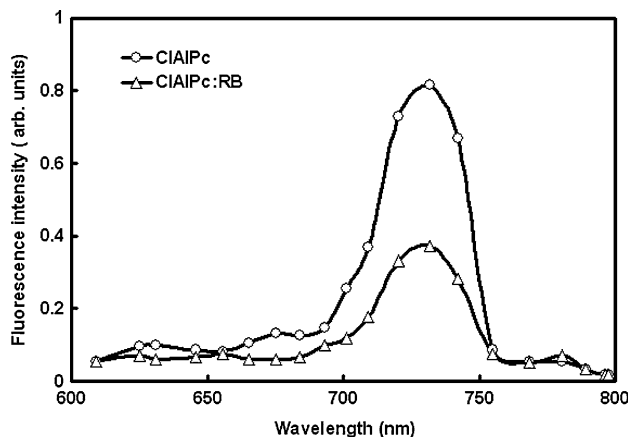


Fig. 6 FL of CIAIPc and CIAIPc:RB thin films

electron affinities of CIAIPc and RB (0.62 eV), which energetically favors the charge transfer process under illumination.

Electrical and photovoltaic properties

Figure 7 shows the current–voltage characteristics of an ITO/CIAIPc:RB/Al device at room temperature in dark and under illumination. The rectification of this device is about 200 at ±0.8 V in dark, while under illumination the reverse bias and forward bias currents are symmetrical. The dark *J–V* characteristics as shown in Fig. 7 for the device consist of three distinct regions:

- (1) a linear region at negative voltages and low forward bias voltages (between –0.5 and 0.5 V where the current is limited by shunt resistance;
- (2) an exponential behavior at intermediate region in forward bias voltages where current is controlled by diode, and

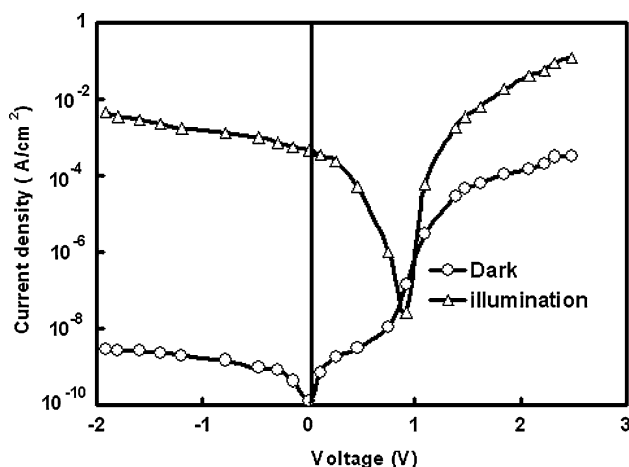


Fig. 7 Current–voltage characteristic in dark and under illumination for ITO/CIAIPc:RB/Al device

- (3) a linear region at high voltages where the current is limited by the series resistance.

The current–voltage characteristics in dark were fitted by standard one-diode model given by

$$J = J_o \left[\exp\left(\frac{q(V - JR_s)}{nkT}\right) - 1 \right] + \frac{q(V - JR_s)}{R_{sh}} - J_{ph}, \quad (2)$$

where J_o is the saturation current density, q the electronic charge, n the diode quality factor, kT the thermal energy, R_s and R_{sh} are the series and shunt resistance, respectively.

Although the specific physical processes in organic semiconductors may be different but the principal loss mechanisms are same, because of that, we can apply the one-diode model to describe the *J–V* characteristics for present device as employed by other researchers [20, 43]. The exponential behavior of the device is attributed to the interface existing as in the case of schottky barrier and bi-layer devices. However, for the devices consisting of an intimate mixture of two materials, a well-defined interface for a charge separation such as p–n junction is not formed. In this case, the D–A interface is spread throughout the bulk sandwiched between two electrodes. Two materials are arranged like a bi-layer, connect the electrodes as a pure phase, or one material is completely enclosed by the other. The exponential behavior of *J–V* characteristics depends on the properties of two materials involved. The slope of *J–V* characteristics in exponential region depends on two parameters, i.e., ideality factor (n) and reverse saturation current (J_o). The ideality factor gives information about the recombination process. The second parameter that affects the exponential part of *J–V* characteristics is the saturation current which gives the numbers of charges able to overcome the energetic barrier in reverse bias.

Since, the quantum efficiency for charge separation in pristine organic semiconductor is low; hence, it is necessary to use the blend of semiconductors with appropriate electron affinities and work functions [44] to overcome the quantum efficiency for charge separation. This so-called D–A principle is successfully applied in liquid-electrolyte and solid-state dye sensitized solar cells as well as polymer/fullerene solar cells. Mixing of acceptor with donor into a composites active layer completely modifies the nature of the thin film devices hence the V_{oc} of these devices. In the case of Ohmic contacts, the negative and positive match the LUMO level of the acceptor and HOMO level of the donor is expected. The maximum V_{oc} for this case will be $(V_{oc})_{max} = E_{Lumo}(A) - E_{homo}(D)$ and this governs the bulk material properties, as part from the difference between the work functions of the positive and the negative electrodes. The work function of ITO matches the HOMO level of CIAIPc resulting in an ohmic contact for

holes in the BHJ solar cells. In BHJ with Ag contact band bending occurs at both interfaces and Eq modifies to

$$q(V_{oc} + \Delta V_b) = (E_{LUMO(A)} - E_{HOMO(D)}), \quad (3)$$

where ΔV_b is the sum of the voltage losses at each contact due to band bending. This equation shows that for two Ohmic contacts the V_{oc} is given by the difference between the HOMO level of the donor and LUMO level of the acceptor, minus the voltage drop losses at these contacts due to band bending. The experimental value of V_{oc} is less than the theoretical value of V_{oc} . This reduction in V_{oc} is caused by the dark current–voltage curve of the diode, which is determined by the ideality factor and the reverse dark current J_o of the diode. In addition to that, a smaller part of V_{oc} loss originates from the fact that the photocurrent in bulk heterojunction device is dominantly field driven.

Dissociation of charge carrier at CIAIPc/RB interface

Organic semiconductors are characterized by low relative dielectric constant typically ranging from 2 to 4, which results a strong Coulomb binding energy (0.5 eV) for the photogenerated electron and hole at the D–A interface. It is well known that in molecular solids, the photogeneration of charge carriers results from the field and temperature-assisted dissociation of singlet excitons [45, 46]. In the present device, we have observed a strong FL quenching and the photoaction spectra of the device closely matches with the optical absorption of blend layer, which leads to generation of free charges in a two-step process: in the first step, coulombically bound germinate electron hole pairs are formed, and secondly the pairs are dissociated into free carriers [47].

In the case of an ideal solar cell, with no recombination or space charge formation, the photocurrent is a direct measurement of the photogenerated charge carriers. In that case, the internal field in the device is given by $E = (V_{oc} - V)/L$, where V is the applied voltage, V_{oc} the open circuit voltage, and L is the thickness of the photoactive layer used in the solar cell. The photocurrent through the external circuit is given by [48]

$$J_{ph} = qGL, \quad (4)$$

where G is the generation of electron and hole pairs. Therefore, for constant generation rate G , J_{ph} is independent of applied field. As a result, in this case the photocurrent given by Eq. 4 is independent of the mobility of either electron or holes and direct measurement of G , because of weaker recombination, the carrier lifetime will always exceed the transit time. However, Sokel and Hughes [49] pointed out that Eq. 4 is not valid for low bias voltages because the diffusion currents have been not

included. Using same approximation which was used for Eq. 4, but including the diffusion process, the photocurrent is given by

$$J_{ph} = qGL \left[\frac{\exp(qV/kT) + 1}{\exp(qV/kT) - 1} - \frac{2kT}{qV} \right], \quad (5)$$

where qGL is the saturated photocurrent.

Interpretation of J – V characteristics for organic solar cells often done by using models developed for inorganic p–n junctions [50, 51]. However, in such cases, no detailed description of electric field distribution and carriers densities in bulk heterojunction solar cells has been included. Baker et al. [52] have proposed a numerical model describing the J – V characteristics of bi-layer OPV devices, which include the dissociation of excitons at D–A interface. Since, the electronic structures of bi-layer and bulk heterojunction are different; therefore, their operational principles are fundamentally different.

Our device can be described by using the metal–insulator–metal picture as employed for other organic solar cells [53]. This means that the device is built up by one semiconductor with the LUMO of the acceptor and HOMO of the donor as conduction and valence band, respectively. The energy difference between LUMO of the acceptor and the HOMO of the donor components can be treated as the effective band gap (E_{gap}) of photoactive blend. In organic semiconductors, the band gap is not rigorously defined quantity due to the Gaussian density of states of both the acceptor and the donor materials [54]. We have described our experimental results employing a model that includes drift and diffusion of charge carriers, and the effect of space charge on the electric field in the device as proposed for polymer: fullerene bulk heterojunction [55, 56]. We have already reported that the current in CIAIPc-based device shows quadratic dependence on voltage [57]. This behavior is occurrence of SCLC enables us to directly determine the hole mobility from the J – V characteristics.

In Fig. 8, the experimental data obtained from the J – V measurements performed on the device are displayed. In this graph, the effective photocurrent density J_{ph} obtained from subtracting the dark current from the current under illumination is plotted as a function of effective applied voltage ($V_o - V$), where V_o is compensation voltage at which $J_{ph} = 0$ [58]. In this way, $V_o - V$ reflects the internal electric field in the device. It is observed that for low effective voltages, the photocurrent increases linearly with effective voltage and subsequently tends to saturate. At low voltages, it can be described with an analytical model developed by Sokel and Hughes for zero recombination as indicated in Fig. 8. This linear behavior at low effective voltage is the result of a direct competition between diffusion and drift currents. At higher effective voltages, all free charge carriers are extracted and the

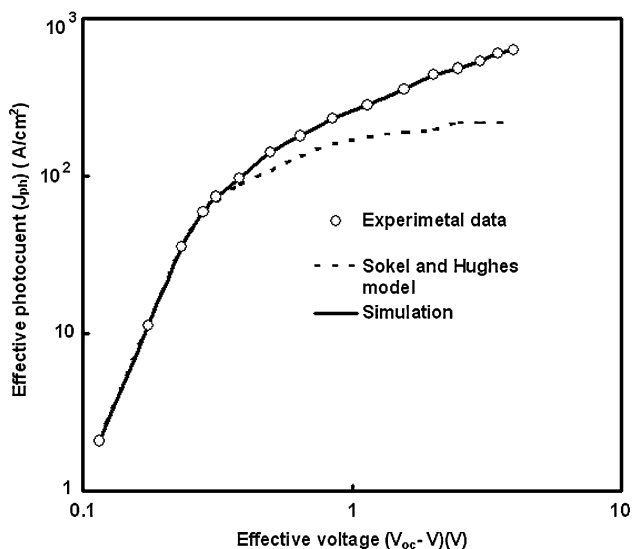


Fig. 8 Effective photocurrent density (J_{ph}) as function of effective applied voltage ($V_{oc} - V$) for the CIAIPc:RB device

photocurrent saturates at qGL . As can be seen from Fig. 8, that the experimentally measured photocurrent does not saturates at qGL , but gradually increases for larger effective voltages that may be attributed to the field dependence of the generation rate G .

We have simulated the J_{ph} using the model developed by Koster et al. [55], which includes the effects of space charge and recombination. In Fig. 8, a fit to the experimental data is shown covering a large effective voltage range. The parameters used in this fit are listed in Table 2.

The external photocurrent becomes saturated when all photogenerated free electrons and holes are extracted from the semiconductor. This implies that the mean electron and hole drift lengths $d_{e(h)} = \mu_{e(h)}\tau_{e(h)} E$ are equal or longer than the thickness of the active layer L , where $\mu_{e(h)}$ is the mobility of electrons (holes), $\tau_{e(h)}$ the lifetime of electron (hole), and E the internal field. In this case no recombination occurs and saturated photocurrent density is given by Eq. 4. However, if either, $d_e < L$, $d_h < L$ or both are smaller than L . Space charge will form and recombination

Table 2 Parameters used in the fit to the data as shown in Fig. 8

Parameter	Numerical values
Band gap of active material (E_g) (eV)	0.98
Electron mobility (μ_e) (m^2/Vs)	8.5×10^{-6}
Hole mobility (μ_h) (m^2/Vs)	1.2×10^{-8}
Effective density of states (N_v) (m^{-3})	10^{25}
Generation rate (G) (m^{-3})	2.0×10^{27}
Dielectric constant (ϵ_r)	3
e/h pair distance (a) (nm)	1.3
Decay rate (k_r) (s^{-1})	2.3×10^6

of free charge carriers becomes significant. In a bulk heterojunction, the excitons are generated uniformly throughout the active layer due to the intermixing of donor and acceptor species and the charge transport is strongly unbalanced since $d_e \neq d_h$. The difference in d_e and d_h originates from a difference in the charge carrier mobility μ_e and μ_h . In CIAIPc:RB blend, the electron mobility of electron is higher than hole mobility and $d_h < L$, the holes will accumulate to a greater extent in the device than the electrons results the nonuniform distribution of applied field. As a consequence, the electric field increases the region near the anode, enhancing the extraction of holes. However, in the region near the cathode, the electric field decreases, diminishing the extraction of electrons. Due to this effect, in the region near the anode, the accumulated holes are not neutralized by an equal density of electrons, which results in a buildup of positive space charge. The electrostatic limit of hole accumulation is reached when the photocurrent generated in this region, $J_{ph} = qGL_1$, where L_1 is the thickness of the space charge layer near the anode, is equal to SCLC [48].

$$J_{SCL} = \left(\frac{9}{8}\right) \epsilon_0 \epsilon_r \mu_h \left(\frac{V^2}{L_1^3}\right), \tag{6}$$

where $\epsilon_0 \epsilon_r$ is the dielectric permittivity. By equating qGL_1 with Eq. 6, it follows that the photocurrent that can be extracted from the device when space charge is formed near the anode is given by [48]

$$J_{ph} = q \left(\frac{9\epsilon_0 \epsilon_r \mu_h}{8q}\right)^{1/4} G^{3/4} V^{1/2}. \tag{7}$$

According to Eq. 7, the SCL photocurrent scales with a 3/4 power dependence on light intensity, while in the absence of space charge, the photocurrent is scaled linearly with the light intensity.

Figure 9 shows, in a double-logarithmic plot, the experimental J_{ph} as a function of incident light intensity for two different voltages, at $V_o - V = 0.1$ V in a square root region and at $V_o - V = 2$ V in the saturated region. The slope S determined from the linear fit to experimental data is about 0.78 and 0.92 in square root and saturation part, respectively. The 1/2 power dependence of J_{ph} on voltage and 3/4 dependence on light intensity is a strong indication for the occurrence of a space charge limited photocurrent in the CIAIPc:RB system.

Effect of thermal annealing

It is reported that the electron and hole mobilities in the blend can be determined from the current–voltage measurements by using electrodes that either suppress the injection of electrons and holes, resulting in hole or

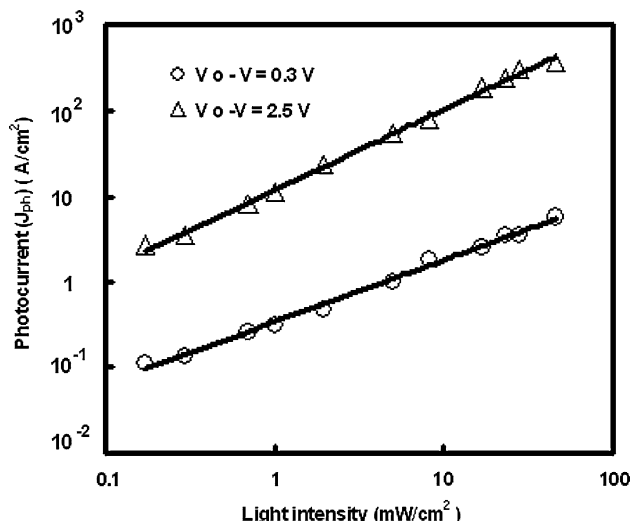


Fig. 9 Incident light intensity dependence of the photocurrent J_{ph} at different effective voltage ($V_o - V$)

electron only devices, respectively [59, 60]. We have applied this technique to measure either the hole or the electron current in the blend of CIAIPc:RB for as-cast and annealed films. In order to fabricate the hole only devices, Au was evaporated as the top electrode to form the ITO/CIAIPc/Au structure. The work function of ITO matches with the HOMO of CIAIPc (4.9 eV) forming nearly Ohmic contact for hole injection, whereas Ag strongly suppresses the electron injection into RB owing a large mismatch between its work functions. A schematic diagram of a hole only device is shown in Fig. 10a. In order to suppress the hole injection into CIAIPc, the bottom electrode must have a low work function. We have fabricated the electron only

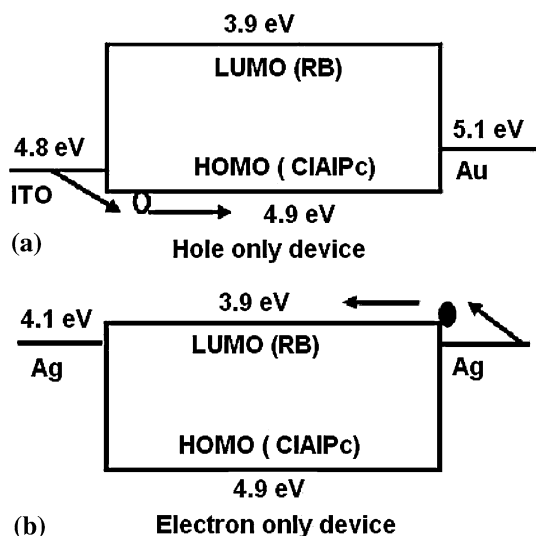


Fig. 10 Schematic diagram of (a) hole only and (b) electron only device

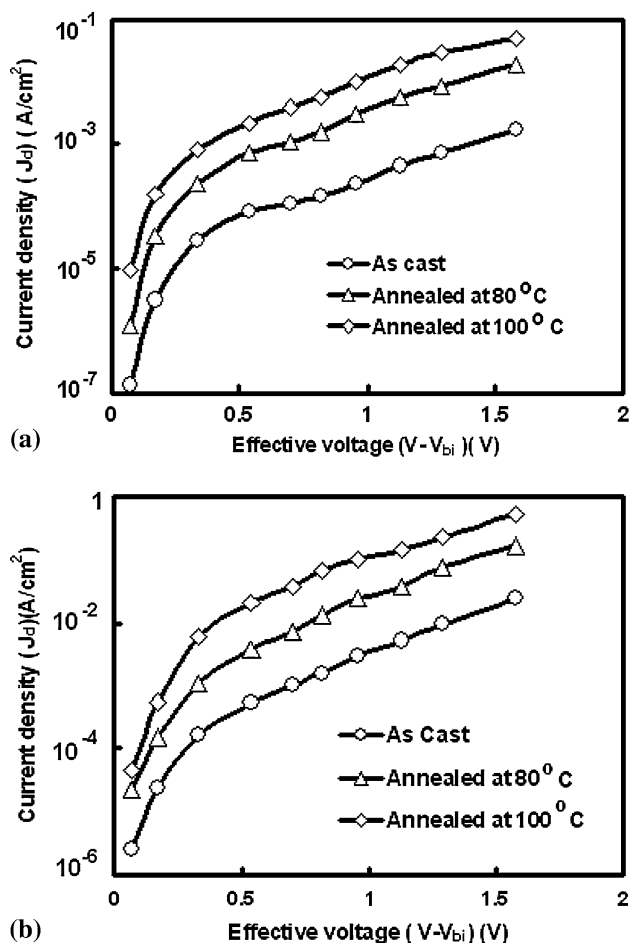


Fig. 11 (a) Variation of dark current density with effective applied voltage ($V - V_{bi}$) of CIAIPc:RB blend devices in hole only configuration. (b) Variation of dark current density with effective applied voltage of CIAIPc:RB blend devices in electron only configuration

devices for the CIAIPc:RB blends having the structure Ag/CIAIPc:RB/Ag as shown in Fig. 10b.

Figure 11a and b shows the experimental dark current densities (J_d) of CIAIPc:RB blends that were measured in hole only and electron only devices, respectively, for different annealing temperatures. The applied voltage is corrected for the built in voltage (V_{bi}). When the applied voltage is greater than V_{bi} , the dark current (J_d) in all devices scales quadratically with voltage which is an indication of SCL transport in the device. This observation is common for low mobility, disordered semiconductors and it allows for a direct determination of the mobility [59–61]. For the electron and hole only devices, the SCL current is given by [62]

$$J_{e(h)} = (9/8)\epsilon_0\epsilon_r\mu_{e(h)} \exp\left(0.891\gamma_{e(h)}\sqrt{V/L}\right) \frac{V^2}{L^3}, \quad (8)$$

where $J_{e(h)}$ is the electron(hole) current, $\mu_{e(h)}$ the zero-field mobility of the electrons and (holes), $\gamma_{e(h)}$ the field

Table 3 Effect of thermal annealing on the hole and electron mobilities in the blend

Mobility (m ² /Vs)	Pure CIAIPc		CIAIPc:RB	
	As-cast	Annealed at 100 °C	As-cast	Annealed at 100 °C
Hole	1.2 × 10 ⁻⁸	5.6 × 10 ⁻⁸	1.2 × 10 ⁻¹⁰	3.8 × 10 ⁻⁸
Electron	–	–	1.6 × 10 ⁻⁷	3.4 × 10 ⁻⁷

activation factor, ϵ_0 the permittivity of free space, ϵ_r the relative permittivity of the material, and L is the thickness of the active layer. The experimental data in figure were fitted using Eq. 8 and the results are shown by the solid lines. We have calculated zero-field mobility of electrons and holes using Eq. 8 in blend of CIAIPc:RB devices both for as-cast, annealed 100 °C and are listed in Table 3. For comparison, the hole mobility of pure CIAIPc, measured under the same experimental, is also shown in Table 3. It is observed that the hole mobility in pure CIAIPc is not affected by thermal annealing. In contrast, the hole mobility of CIAIPc in the blend is strongly affected by the presence of RB and it drops almost two orders of magnitude for as-cast device. However, the mobility of the holes increases upon thermal annealing and its value is approximately equal to that for pure CIAIPc, when the device is annealed at 100 °C. It is also observed that the field activation factor decreases upon the thermal annealing. Moreover, the electron mobility of RB in the blend is also affected by thermal annealing. In the as-cast device, the difference in the hole mobility of CIAIPc and electron mobility of RB is quite large, but this difference is reduced as the device is annealed. As a result, the charge transport is the as-cast film that is strongly unbalanced and the current is fully dominated by the electrons. Upon thermal annealing, slow crystallization of CIAIPc takes place and de-mixing between CIAIPc and RB takes place, which leads to an enhanced charge transport. As a result, interpenetrating networks composed of CIAIPc crystals and aggregated RB rich domains are formed, which provide continuous pathways in the entire photoactive layer for efficient electron and hole transport. As the difference in the mobilities of electron and hole is reduced upon thermal annealing which leads to a balanced charge transport in the device.

The absorption spectra of CIAIPc:RB mixture were investigated before and after thermal annealing and shown in Fig. 12. The intensity of absorption peaks for CIAIPc:RB blend is slightly less than that for CIAIPc (Fig. 3). This might be originated from broken conjugation in the presence of the RB, resulting in segments with a shorter conjugation length and weaker inter-chain interaction. It is observed that the absorption peak attributed to CIAIPc

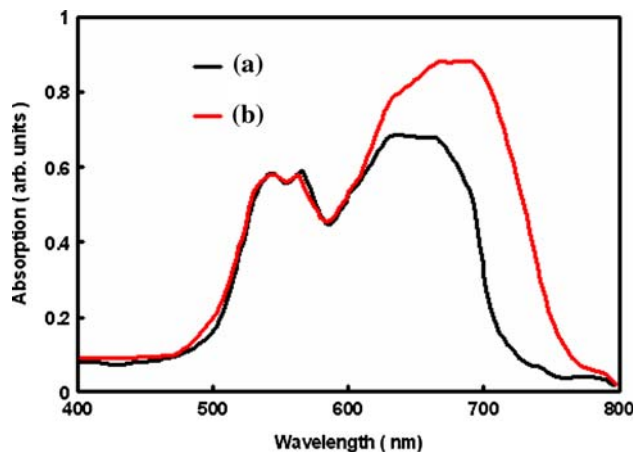


Fig. 12 Absorption spectra of CIAIPc:RB blend films (a) as-cast (b) annealed at 100 °C

shows a pronounced red-shift upon thermal annealing (shift in Q-band from 680 to 700 nm), while the peak of RB remains unchanged. Upon thermal annealing, the RB de-mixes from the CIAIPc, thereby increasing the degree of crystallinity of the CIAIPc and consequently undergoes a noticeable red-shift approaching the spectrum of CIAIPc. The overall effect of the red-shift of the optical absorption upon thermal annealing, with respect to as-cast film, is so that it improves the spectral overlap with solar emission, resulting in an increased absorption by the active layer.

Figure 13 shows the experimental photocurrent (J_{ph}) of ITO/CIAIPc:RB/Ag device is a double logarithmic plot as a function of effective voltage. The curves correspond to different postproduction treatments: as-cast, thermally annealed at 100 °C. Table 4 also shows the photovoltaic parameters for annealed device. The open circuit voltage slightly decreases upon thermal annealing. Conversely, all other device parameters increase upon thermal annealing.

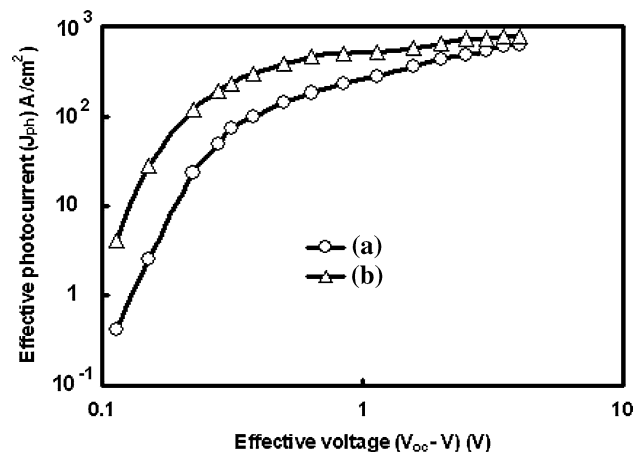


Fig. 13 Effective photocurrent (J_{ph}) as a function of effective applied voltage for Ag/CIAIPc:RB/ITO device (a) as-cast and (b) annealed at 100 °C device

Table 4 Photovoltaic parameters calculated from J – V characteristics under illumination

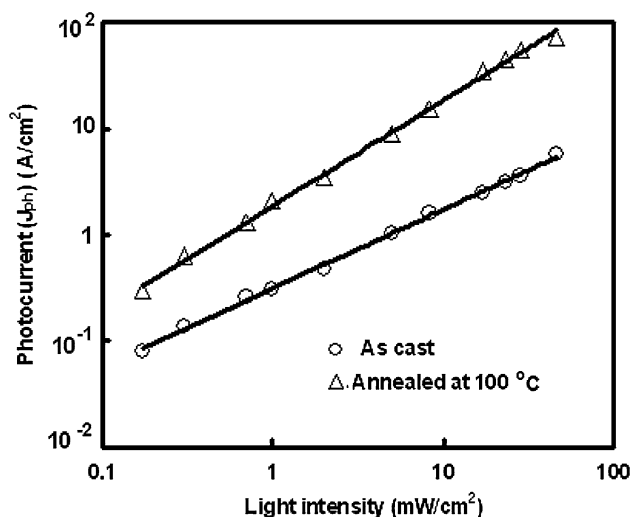
Parameters	ITO/ CIAIPc/Ag	ITO/ CIAIPc: RB/Ag	ITO/ CIAIPc:RB/Ag (Annealed at 100 °C)
J_{sc} (mA/cm ²)	0.034	0.44	1.56
V_{oc} (V)	1.04	0.92	0.89
FF	0.32	0.48	0.54
Power conversion efficiency (η)	0.011	0.20	0.75

The enhancement in the power conversion efficiency as a result of thermal annealing of photoactive layer is due to the increase in charge carrier mobility induced by better crystallization of the CIAIPc and an improved overlap with the solar emission occur. The increase in the short-circuit photocurrent is due to the enhanced hole mobility of CIAIPc and consequently the difference between the electron and the hole mobilities is reduced.

We have studied the light intensity dependence of effective photocurrent in the low-voltage region for both as-cast device and device annealed at 100 °C and shown in Fig. 14. The photocurrent (J_{ph}) follows the power law dependence as given by

$$J_{ph} = P_{light}^S, \quad (8)$$

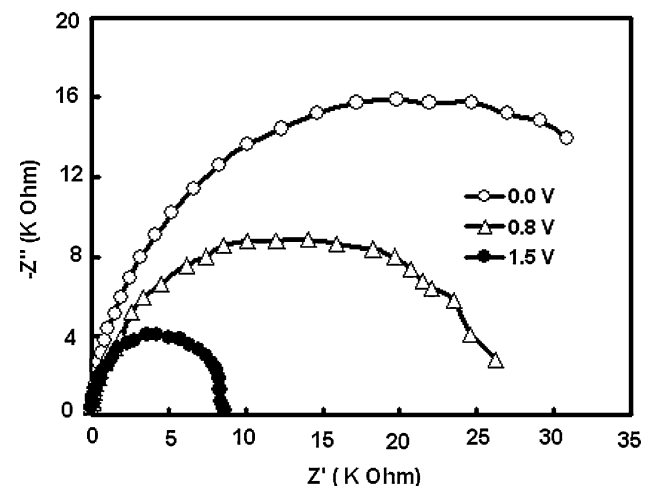
where P_{light} is the intensity of light and exponent S is 0.72 and 0.98 for as-cast device and device annealed at 100 °C, respectively. This indicates that the photocurrent is SCLC for as-cast device, whereas the photocurrent is space charge free limit for annealed one [63]. It can be seen from Fig. 13 that there is no square law dependence of photocurrent is

**Fig. 14** Light intensity dependence of photocurrent at effective voltage of 0.3 V for as-cast and annealed device

observed when the device is annealed at 100 °C. This indicates that the photocurrent becomes space charge free upon thermal annealing resulting increased hole mobility in CIAIPc, leading to a better balanced charge transport. The absence of space charge effects is further evidenced by almost linearly ($S = 0.98$) dependence of J_{ph} on P_{light} . Therefore, the enhancement in the device efficiency upon thermal annealing is mainly a result of the improved hole mobility in CIAIPc inside the blend and light harvesting. With the increased hole transport, the device recovers from the space charge limitation to become space charge free, balanced transport. The absence of square root dependence of photocurrent on effective voltage in the device annealed at 100 °C leads to a strong enhancement of both fill factor (FF) and short circuit current (J_{sc}).

Impedance spectroscopy

Cole–Cole plots of the variation of imaginary impedance $\text{Im}(Z)$ with real impedance $\text{Re}(Z)$ under different biasing voltages at room temperature are shown in Fig. 15 for the ITO/CIAIPc:RB/Ag device, wherein the frequency increases from right to left (100 Hz to 1 MHz). This figure shows the pronounced voltage dependence of the device impedance in the low-frequency range. At high-frequency region, the impedance is almost independent of bias voltage. Figure 16 shows Cole–Cole plots for the ITO/CIAIPc:RB/Ag device, under different temperature at zero biasing voltage. This figure also shows the pronounced temperature dependence of the device impedance in the low-frequency range. At high-frequency region, the impedance is almost independent of bias voltage. In Figs. 15 and 16, the variations of $\text{Im}(Z)$ with $\text{Re}(Z)$ display a one symmetric semicircle attributable to a bulk heterojunction between RB and CIAIPc layers. A single semi-circle in a Cole–Cole plot

**Fig. 15** Cole–Cole plot for ITO/CIAIPc:RB/Ag device at room temperature for different biasing voltages

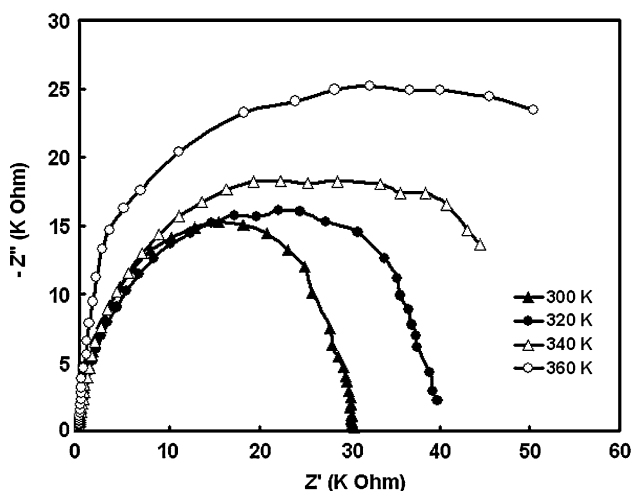


Fig. 16 Cole–Cole plots for ITO/CIAIPc:RB/Al device at different temperatures

suggests a single relaxation time of the equivalent circuit, and the results could be fitted using a parallel combination of a resistor and capacitor.

We have studied the impedance spectroscopy of the devices to obtain relative effect of exciton dissociation and charge transport of the carrier in the devices. The measurements were carried out in dark and under illumination for as-cast device and device annealed at 100 °C. The plots between real and imaginary components of complex impedance for both devices are shown in Fig. 17. For each device, the radius in these plots represents the bulk resistance of the device and found this decreases when the device is illuminated. It can be seen from Fig. 17 that the change in the bulk resistance is more in annealed device as compared to as-cast device. Hence, the change in the bulk resistance has a direct relevance with the photocurrent and power conversion efficiency. We have calculated the relative dielectric

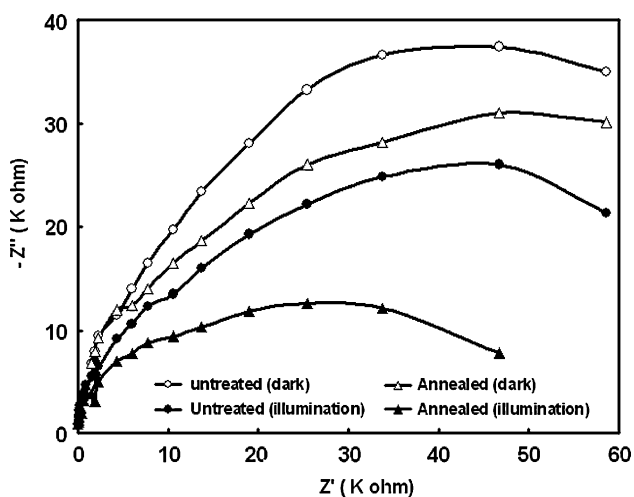


Fig. 17 Cole–Cole plots for untreated and annealed device

constant of the blend (both for as-cast and annealed) from the impedance spectroscopy in dark as well as under illumination. It is found that at higher frequencies, the dielectric constant of the blend remains almost unchanged under illumination. Under illumination, at low frequencies, the dielectric constant increases on illumination and the degree of increase is different for as-cast and annealed devices. Since, the dielectric properties are sensitive to the charge separation and their movement in the device. The operation of photovoltaic device involves these mechanisms; therefore, the relation amongst change in dielectric constant, change in bulk resistance and photocurrent is significant. It is observed that the degree of change in both bulk resistance and dielectric constant under illumination is more for annealed device than that for as-cast device, which is related with the higher photocurrent in the annealed device. The increase in dielectric constant under illumination can be explained in terms of drifting of electrons and holes toward Ag and ITO electrodes, respectively, resulting increase in the capacitance of the device. Hence, the degree of the change in dielectric constant and internal bulk resistance may be the measure of the efficient exciton dissociation and their transfer to respective collecting electrodes.

Conclusions

The blend of CIAIPc and RB has been investigated as photoactive material for potential application in photovoltaic device. Optical absorption and FL of blend, current–voltage (*J–V*) characteristics in dark and under illumination, and impedance spectroscopy have been carried out for performance evaluation of device. The fluorescence quenching of CIAIPc when mixed with RB indicates the formation of bulk heterojunction with increased interfacial area, which leads to an efficient photo-induced charge transfer between donor and acceptor. The experimental *J–V* characteristics are interpreted using a model, which include the drift, diffusion of charge carriers, and the influence of space charge on the electric field and temperature-dependent generation of free carriers transport. Both absorption peak as well as absorption edge shifts toward the longer wavelength region and height of the absorption peak also increases upon thermal annealing. This indicates the RB demixes from CIAIPc, thereby increasing the degree of crystallinity of the CIAIPc which leads to an enhanced charge transport and improved light harvesting. The power conversion efficiency of the device was increased by almost one order of magnitude when the device was annealed at 100 °C. The most important factor in obtaining high efficiency was found to be the enhancement in the hole mobility in CIAIPc phase of the blend, relative to the as-cast device. For as-cast devices, the difference in electron–hole

transport in the blend is too large and photocurrent is strongly limited by the buildup of space charge. The difference in electron and hole mobilities in RB and CIAIPc phase in the blend, respectively, is reduced upon thermal annealing and, consequently, the space charge no longer limits the performance of the device. Based on the mobility and photocurrent measurements, we conclude that the effect of thermal annealing on the performance is understood to be due to higher exciton generation and their subsequent dissociation into free carriers and increase in hole mobility which results in balanced charge transport.

Additionally, the impedance properties in dark and under illumination showed that change in bulk resistance and dielectric constant of the blend had a direct relation with the photocurrent generation in the device.

Acknowledgement We are grateful to Council for Scientific and Industrial Research for financial support through project.

References

- Spanggaard H, Krebs FC (2004) *Sol Energy Mater Sol Cells* 83:125. doi:10.1016/j.solmat.2004.02.021
- Sun SS, Sariciftci NS (2005) *Organic photovoltaic mechanisms, materials, devices*. CRC Pres, Boca Ration
- Hoppe H, Sariciftci NS, Meissner D (2002) *Mol Cryst Liq Crystallogr* 385:113. doi:10.1080/713738799
- Hoppe H, Sariciftci NS (2004) *J Mater Chem* 19:1924
- Singh B, Sariciftci NS (2006) *Annu Rev Mater Res* 36:199. doi:10.1146/annurev.matsci.36.022805.094757
- Krebs FC, Spanggaard H (2005) *Chem Mater* 17:5235. doi:10.1021/cm051320q
- Ma W, Yang C, Gong X, Lee K, Heeger AJ (2005) *Adv Funct Mater* 15:1617. doi:10.1002/adfm.200500211
- Wang XJ, Perzon E, Delgado JL, Dela Cruz P, Zeng FL, Langa F et al (2004) *Appl Phys Lett* 85:5081. doi:10.1063/1.1825070
- Wang X, Perzon E, Oswald F, Langa F, Admassie S, Anderson MR et al (2005) *Adv Funct Mater* 15:1665. doi:10.1002/adfm.200500114
- Yu G, Gao J, Hummelen JC, Wudl F, Heeger AJ (1995) *Science* 270:1789. doi:10.1126/science.270.5243.1789
- Halls JJM, Walsh CA, Greenham NC, Marseglia EA, Friend RH, Morattia SC et al (1995) *Nature* 376:498. doi:10.1038/376498a0
- Peumens P, Yakimov A, Forrest SR (2003) *J Appl Phys* 93:3693. doi:10.1063/1.1534621
- Hong ZR, Lee CS, Lee ST, Li WL, Shirota Y (2002) *Appl Phys Lett* 81:2898
- Rand BP, Xue J, Uchida S, Forrest SR (2005) *J Appl Phys* 98:124902. doi:10.1063/1.2142072
- Scharber MC, Muhlbacher D, Koppe M, Denk P, Waldauf C, Heeger AJ et al (2006) *Adv Mater* 18:789. doi:10.1002/adma.200501717
- Heggie DA, MacDonald BL, Hill IG (2006) *J Appl Phys* 100:104505. doi:10.1063/1.2374694
- Bundaagd E, Krebs FC (2007) *Sol Energy Mater Sol Cells* 91:954. doi:10.1016/j.solmat.2007.01.015
- Koeppe R, Bossart O, Calzaferri G, Sariciftci NS (2007) *Sol Energy Mater Sol Cells* 91:986. doi:10.1016/j.solmat.2007.01.008
- Gunes S, Neugebauer H, Sariciftci NS (2007) *Chem Rev* 107:1324. doi:10.1021/cr050149z
- Waldauf C, Scharber MC, Schilinsky P, Hauch JA, Brabec CJ (2006) *J Appl Phys* 99:104503. doi:10.1063/1.2198930
- Shin WS, Jeong HH, Kim MK, Jin SH, Kim MR, Lee JK et al (2006) *J Mater Chem* 16:384. doi:10.1039/b512983d
- Padinger F, Rittberger R, Sariciftci NS (2003) *Adv Funct Mater* 13:85. doi:10.1002/adfm.200390011
- Drees M, Premaratne K, Graupner W, Heflin JR, Devis RM, Marciu D, Miller M (2002) *Appl Phys Lett* 81:4607. doi:10.1063/1.1522830
- Hiramoto M, Suegaki M, Yakoyama M (1990) *Chem Lett* 19:327. doi:10.1246/cl.1990.327
- Suemori K, Miyata T, Yokoyama M, Hiramoto M (2005) *Appl Phys Lett* 86:063509. doi:10.1063/1.1863451
- Uchida S, Xue J, Rand BP, Forrest SR (2004) *Appl Phys Lett* 84:4218. doi:10.1063/1.1755833
- Schultes SM, Sullivan P, Heutz S, Sanderson M, Jones TJ (2005) *Mater Sci Eng C* 25:858. doi:10.1016/j.msec.2005.06.039
- Gebeyehu D, Maennig B, Drechsel J, Leo K, Pfeiffer M (2003) *Sol Energy Mater Sol Cells* 79:81. doi:10.1016/S0927-0248(02)00369-0
- Chan MY, Lai SL, Fung MK, Lee CS, Lee ST (2007) *Appl Phys Lett* 90:023504. doi:10.1063/1.2430783
- Balaban TS (2005) *Acc Chem Res* 38:612. doi:10.1021/ar040211z
- Wasielewski MS (1992) *Chem Rev* 92:435
- Harriman A, Sauvage JP (1993) *Chem Soc Rev* 25:198
- Choi MS, Yamazaki T, Yamazaki I, Aida T (2004) *Angew Chem Int Ed* 43:150. doi:10.1002/anie.200301665
- De la Torre G, Nicolau M, Torres T (2001) In: Nalwa HS (ed) *Phthalocyanines, synthesis, supramolecular organization and physical properties*. Academic Press, New York
- De la Torre G, Vazquez P, Agullo-Lopez F, Torres T (2004) *Chem Rev* 104:3723. doi:10.1021/cr030206t
- Gouloumis A, Liu SG, Vazquez P, Echegoyen L, Torres T (2001) *Chem Commun* 399
- de la Escoura A, Martinez-Diaz MV, Guldi DM, Torres T (2006) *J Am Chem Soc* 128:4112. doi:10.1021/ja058123c
- Li Y, Cao Y, Gao J, Wang D, Yu G, Heeger AJ (1999) *Synth Met* 99:243. doi:10.1016/S0379-6779(99)00007-7
- Kulkarni AP, Wu PT, Kwon TW, Jenekhe SA (2005) *J Phys Chem B* 109:19584. doi:10.1021/jp0529772
- Richler MM, Fan FF, Klavettler F, Heeger AJ, Bard AJ (1994) *Chem Phys Lett* 226:115. doi:10.1016/0009-2614(94)00716-0
- Snaith HJ, Arias AC, Morteani AC, Silva C, Friend RH (2003) *Nano Lett* 2:1353. doi:10.1021/nl0257418
- Barth S, Bassler H (1997) *Phys Rev Lett* 79:4445. doi:10.1103/PhysRevLett.79.4445
- Brabec CJ, Cravino A, Zerza G, Sariciftci NS, Kiebooms R, Vanderzande D et al (2001) *J Phys Chem B* 105:1528. doi:10.1021/jp003407z
- Bredas JL, Beljonne D, Coropceanu V, Cornil J (2004) *Chem Rev* 104:4917. doi:10.1021/cr040084k
- Borsenberger PM, Contois LE, Hoesterey DC (1978) *J Chem Phys* 68:637. doi:10.1063/1.435731
- Chance RR, Braun CL (1976) *J Chem Phys* 64:3573. doi:10.1063/1.432707
- Herlel D, Soh EV, Bassler H, Rothberg LJ (2002) *Chem Phys Lett* 361:99. doi:10.1016/S0009-2614(02)00898-9
- Goodman AM, Rose A (1971) *J Appl Phys* 42:2823. doi:10.1063/1.1660633
- Sokol R, Hughes RC (1982) *J Appl Phys* 53:7414. doi:10.1063/1.330111
- Katz EA, Faiman D, Tuladhar SM, Kroon JM, Wienk MM, Fromhertz T et al (2001) *J Appl Phys* 90:5343. doi:10.1063/1.1412270
- Schilinsky P, Waldauf C, Hausch J, Brabec CJ (2004) *J Appl Phys* 95:2816. doi:10.1063/1.1646435

52. Barker JA, Ramadale CM, Greenham NC (2003) *Phys Rev B* 67:075205. doi:[10.1103/PhysRevB.67.075205](https://doi.org/10.1103/PhysRevB.67.075205)
53. Brabec CJ, Sariciftci NS, Hummelen JC (2001) *Adv Funct Mater* 11:15. doi:[10.1002/1616-3028\(200102\)11:1<15::AID-ADFM15>3.0.CO;2-A](https://doi.org/10.1002/1616-3028(200102)11:1<15::AID-ADFM15>3.0.CO;2-A)
54. Bassler H (1993) *Phys Status Solidi B* 175:15. doi:[10.1002/pssb.2221750102](https://doi.org/10.1002/pssb.2221750102)
55. Koster LJA, Smits ECP, Michailetchi VD, Blom PWM (2005) *Phys Rev B* 72:085205. doi:[10.1103/PhysRevB.72.085205](https://doi.org/10.1103/PhysRevB.72.085205)
56. Blom PWM, Michailetchi VD, Koster LJA, Markov DE (2007) *Adv Mater* 19:1551. doi:[10.1002/adma.200601093](https://doi.org/10.1002/adma.200601093)
57. Sharma GD (1995) *Synth Met* 74:227. doi:[10.1016/0379-6779\(95\)03360-V](https://doi.org/10.1016/0379-6779(95)03360-V)
58. Mihailetchi VD, Koster LJA, Hummelen JC, Blom PWM (2004) *Phys Rev Lett* 93:216601. doi:[10.1103/PhysRevLett.93.216601](https://doi.org/10.1103/PhysRevLett.93.216601)
59. Mihailetchi VD, Koster LJA, Blom PWM, Meizer C, De Boer B, van Duren JKJ et al (2005) *Adv Funct Mater* 15:795. doi:[10.1002/adfm.200400345](https://doi.org/10.1002/adfm.200400345)
60. Meizer C, Koop EJ, Mihailetchi VD, Blom PWM (2004) *Adv Funct Mater* 14:865. doi:[10.1002/adfm.200305156](https://doi.org/10.1002/adfm.200305156)
61. Goh C, Kline RJ, McGhee MD, Kadnikova EN, Frechet JMJ (2005) *Appl Phys Lett* 86:122110. doi:[10.1063/1.1891301](https://doi.org/10.1063/1.1891301)
62. Murgatroyd PN (1970) *J Phys D* 3:151. doi:[10.1088/0022-3727/3/2/308](https://doi.org/10.1088/0022-3727/3/2/308)
63. Mihailetchi VD, Wildeman J, Bolm PWM (2005) *Phys Rev Lett* 94:126602. doi:[10.1103/PhysRevLett.94.126602](https://doi.org/10.1103/PhysRevLett.94.126602)